applied sciences

MDPI

Article

Experimental Study on the Damage of Optical Materials by out of Band Composite Laser

Liu Yang [1,*], Liu Lisheng [1], Tang Wei [1], Shao Junfeng [1], Li Xuelei [1], Sun Junjie [1], Shao Ming [2] and Cheng Xiangzheng [2]

1 State Key Laboratory of Laser Interaction with Matter, Changchun Institute of Optics, Fine Mechanics and Physics, Chinese Academy of Sciences, Changchun 130033, China; liuls@ciomp.ac.cn (L.L.); twei222@163.com (T.W.); 13159754836@163.com (S.J.); lixlbox@163.com (L.X.); 15143115236@163.com (S.J.)

2 Key Laboratory of Electro-Optical Countermeasures Test & Evaluation Technology, Luoyang 471003, China; lyshaoming@163.com (S.M.); renxiaoyaocxz_1@163.com (C.X.)

* Correspondence: liuyangdk@ciomp.ac.cn

Received: 25 April 2020; Accepted: 19 May 2020; Published: 21 May 2020

Abstract: For the paper, experimental studies were performed on the damage of the Ge- and Si-based flat window by lasers out-of-band. The experimental results showed that lasers out-of-band can cause film damage and substrate damage to Ge and Si windows. The high-energy laser damage window mechanism mainly manifested as thermal effects. The composite laser damage thresholds for the substrate were an Si window of 21.6 J/cm^2 and a Ge window of 3 J/cm^2. Compared with continuous laser and long pulse laser experimental results, it was found that the use of long pulse-continuous composite constitution could effectively reduce the damage threshold. Compared to the long-pulse laser, the composite laser could achieve similar damage effects with a smaller energy density.

Keywords: flat window; high power composite laser; out of band; laser material interaction; damage effect

1. Introduction

Laser-induced damage to optical components is a key research issue in high-energy laser emission systems, and it is also one of the key technologies that need to be resolved for the development of high-power optoelectronic countermeasure systems. Starting from the basic principle of the interaction between lasers and matter, a laser can interact with optical systems and optical elements through the laser thermal effect and laser–electron interactions. This provides a theoretical basis for a single-band laser to achieve full-band photoelectric loading. Based on this principle, researchers have proposed the concepts of "in-band damage" and "out-band damage." "In-band damage" refers to the damage of an optoelectronic system by a laser in its operating band. Researchers generally believe that the damage mechanism of "in-band damage" comprises the semiconductor band structure theory, thermoelectric effect, etc., and "in-band damage" has been widely used in contemporary optoelectronic countermeasures. "Out-of-band damage" refers to the damage of photoelectric systems by lasers outside the operating band. Earlier studies have suggested that optoelectronic components do not respond or respond weakly to the lasers outside the operating band. However, with the advancement of laser technology, more and more high-power and high-energy lasers have begun to be applied to high-power laser emission systems. This has caused the risk of damage to optical systems by lasers outside the high-energy band. Therefore, it is necessary to carry out systematic experimental research on the interaction between high-energy lasers outside the band and optical elements.

At present, the research reports on "out-band damage" have mainly focused on photodetectors. The related literature has conducted experimental studies on interference and damage of HgCdTe, InSb,

and Si-CCD (charge coupled device) detectors [1–7]. The mainstream view believes that the mechanism of "out-band damage" is mainly the semiconductor band structure theory (CCD) and thermoelectric effects (Mid-wavelength infrared and Long-wavelength infrared). Some researchers have found that out-of-band lasers can also damage window mirrors in experiments of laser interference effects on optical systems. Wang [8] used a Deuterium fluoride laser to perform cumulative damage experiments on a visible light plane array CCD and found that multiple irradiations of the laser at different positions on the CCD surface and multiple irradiations at the same position damaged the K9 (A glass model) optical window. Wang [9] experimented with a 3.8 µm continuous-wave laser to destroy the ternary Photoconductive type HgCdTe detector system and found that the film and substrate damage occurred in the Ge window at the laser irradiation spot; they also found the internal filter had a melting phenomenon. Existing research believes that the key to "out-band damage" lies in whether the laser source has a sufficient damage ability, and the multi-mode composite laser has this characteristic. A multi-mode composite laser consists of lasers with different wavelengths, different systems, and different frequency changes that act on the target at the same time or alternately to obtain a better damage effect than a single continuous-wave or Pulsed-laser. Related studies have been conducted on composite lasers: Cheng [10] carried out an experimental study on the combined damage of a 1030 nm continuous laser and a 1064 nm pulsed laser and found that the "non-linear avalanche ablation" effect occurred under the combined or alternating effects of two lasers, which made the combined laser have a stronger ablation effect than the pulse laser. The experimental results showed that the average single-pulse ablation amount of the composite laser was 13 times that of the pulse laser. Wang [11] found, in a study of pulse-pulse composite lasers, that the increase in target damage was a result of an increased power density. The damage effect of composite lasers is related to the overlap of pulse time domains, and the damaging effect of composite lasers is better than that of long-pulse lasers. Jiao [12], using 1053 nm pulsed and 1064 nm multiple compound lasers to study the irradiation effect of steel found that the surface reflection of steel decreased with the increase of pulsed laser frequency. The pre-irradiation of steel plates with a long pulse laser can increase its absorption rate for subsequent lasering. Xiao [13,14] simulated the thermodynamic characteristics of the continuous-pulse composite laser irradiation of aluminum alloys. Through simulation, it was found that the composite laser could significantly increase the size of the molten pool and increase the center temperature of the irradiation spot. The longer the "preheating" time, the shorter the yield time of the material, the larger the plastic deformation, and the larger the yield range.

According to the analysis of the above literature, it is known that the research on the laser irradiation effects of composite lasers is still in its infancy. Almost all reported studies have used low-energy in-band laser sources. The research targets have mostly been photoelectric sensors and metal structural parts. Composite laser damage studies on optical components have not been reported. For this paper, high-power laser damage experiments were performed on a common Ge-based and Si-based flat window to provide technical support for the design of high-power laser emission systems.

2. Laser Absorption in Optical Elements

2.1. Absorption and Scattering of Optical Film

A flat window is composed of surface optical films and substrates. The following assumptions are used to solve the reflectivity of optical films: The film does not absorb incident light, its refractive index is uniform, and both interfaces are smooth. These assumptions accurately reflect the optical properties of general dielectric films. An optical film made of a single-layer film has a limited optical performance. To meet a variety of optical requirements, multi-layer films are needed. Suppose an optical film composed of an m-layer film—then, the j-layer has a refractive index of n_j, and the feature matrix of this layer of film can be expressed as:

$$A_j = \begin{bmatrix} \cos\delta_j & \mathrm{i}n_i/\sin\delta_j \\ \mathrm{i}n_j\sin\delta_j & \cos\delta_j \end{bmatrix} \quad (1)$$

where $\delta_j = (2r/\lambda)n_j d_j$ is the phase thickness of the j-th layer film. The combined feature matrix of the m-layer film is:

$$\begin{bmatrix} m_{11} & m_{12} \\ m_{21} & m_{22} \end{bmatrix} = \prod_{j=0}^{m} \begin{bmatrix} \cos\delta_j & i n_i / \sin\delta_j \\ i n_j \sin\delta_j & \cos\delta_j \end{bmatrix} \tag{2}$$

where n_0, n_s, and λ are the refractive index of the incident medium, the refractive index of the substrate, and the laser wavelength, respectively. For transparent dielectric films, m_{12} and m_{21} are pure imaginary numbers, and m_1 and m_{22} are pure real numbers. The reflection coefficient r and reflectance R of the multilayer film are:

$$r = \frac{(n_0 m_{11} - n_s m_{22}) + (n_0 n_s m_{12} - m_{21})}{(n_0 m_{11} + n_s m_{22}) + (n_0 n_s m_{12} + m_{21})} \tag{3}$$

$$R = \frac{(n_0 m_{11} - n_s m_{22})^2 + (n_0 n_s m_{21})^2}{(n_0 m_{11} + n_s m_{22}) + (n_0 n_s m_{12} + m_{21})^2} \tag{4}$$

The reflectivity of the optical film can be solved by the above two equations [15–17].

2.2. Temperature Field of Optical Film

The direct factor leading to the destruction of the optical film under laser irradiation is the temperature rise caused by the thermal effect. To study the laser damage of optical film, the time and space distribution of the temperature field of optical film should be considered, and these can be determined by solving the heat conduction equation with the laser source term. The heat conduction equation of a multilayer dielectric film and its initial and boundary conditions can be expressed as:

$$\left.\begin{array}{l} c_i \dfrac{\partial}{\partial t} T_i(r,z,t) - k_i \nabla^2 T_i(r,z,t) = g_i(r,z,t) \\ \dfrac{\partial}{\partial z} T_1(r, z=0, t) = H T_1(r,0,t) \end{array}\right\} i = 1, 2, \ldots \tag{5}$$

Boundary conditions: $r \to \infty$ or $z \to \infty$:$T \to 0$

Initial conditions: $T_i(r,z,0) = T_0(r,z)$

Among them, c_i and k_i are the specific heat capacity and thermal conductivity of the i-th layer film, respectively; H is the surface heat exchange constant, which is related to the surface thermal radiation and thermal convection; and g_i is the laser energy deposited in the i-th film:

$$g_i(r,z,t) = \frac{\partial^3 p_i(r,z,t)}{\partial r \partial z \partial t} \tag{6}$$

where $P_i(r,t,z)$ is the Poynting vector of the i-th film. The energy transmission between the membrane layers meets the principles of temperature continuity and heat flow balance ($i = 1, 2, \ldots$) leads to:

$$\begin{aligned} &T_i(r,z_i,t) = T_{i+1}(r,z_i,t), \\ &\left(\frac{T_i - T_{i+1}}{R_i}\right)_{z=z_i} = \left(\frac{T_{i+1} - T_{i+2}}{R_{i+1}}\right)_{z=z_{i+1}} \end{aligned} \tag{7}$$

where R_i is the thermal resistance at the interface between the i and $i + 1$ films, z_i and z_{i+1} are the positions of the interface, and T_i and T_{i+1} are the temperatures of the two films at the corresponding interfaces. Solving the equations provides the temperature distribution of the optical film [17–20].

2.3. Optical Element Substrate Thermal Response

The steady system assumes that the semiconductor material is crystal and its internal heat conduction may be anisotropic. The crystal structure of semiconductor materials such as silicon germanium is a cubic crystal system, and the thermal conductivity of this crystal structure is the

spherical tensor. It can be considered that the specificity of heat conduction in the same characteristic material is the same [21,22].

The expression of the heat flux density vector can be obtained from Fourier's law:

$$q = -k_{ij}\frac{\partial T}{\partial x_j}e_i \tag{8}$$

where K_{ij} is the thermal conductivity coefficient component; x_j (j = 1,2,3) is the coordinate in the xyz direction; and ei is the basis vector in the xyz direction.

Bring Equation (1) into the heat flux density expression to obtain the heat conduction equation in the semiconductor material:

$$k_{ij}\frac{\partial^2 T}{\partial x_i \partial x_j} + g = \rho c_p \frac{\partial T}{\partial t} \tag{9}$$

where ρ is the density and c_p is the specific heat capacity at constant pressure.

The heat flux density of the laser incident surface is:

$$\left.\frac{\partial T}{\partial x}\right|_{x=0} = \eta I_0 \tag{10}$$

The incident laser has a Gaussian distribution, as follows:

$$I(r) = I_0 \cdot e^{-r^2/\omega^2} \tag{11}$$

where I_0 is the incident power density, r is the distance from the reference point to the center of the spot, and w is the spot radius.

Convection heat transfer on the rear surface of the target is expressed as:

$$-k\left.\frac{\partial T}{\partial x}\right|_{x=L} = h[T(L,t) - T_\infty] \tag{12}$$

According to Equations (8)–(12) can solve the temperature distribution $T(x, t)$ of a flat window under the action of a laser [23–25]. Due to the non-linear changes in the actual physical parameters, the temperature field is also unstable. Therefore, the finite element calculation method can be used to calculate the temperature distribution of a flat window under the action of a laser over time.

3. Experimental Study of Composite Laser Damaged Flat Window

A composite laser damage effect experimental platform was set up, as shown in Figure 1. The continuous and pulsed laser triggering was controlled by a digital delay pulse generator, and the laser parameters were monitored online by a spectroscope. Before starting the experiment, we used the coaxial indicating light to fix the spot position on the flat window. When ready, we used the digital delay pulse generator to control laser delay and trigger. During the experiment, the laser status was monitored with a beam quality analyzer and a power meter. The laser irradiation time was 5 s, and the average value was recorded by repeating the experiment ten times for each power and energy value. The experimental observation system consisted of a visible high-speed camera, an infrared thermal imager, and a plasma spectrometer. We determined whether the window was damaged according to the temporal and spatial distribution of the spot collected by the plasma spectrometer. We used the photodetector to monitor the window mirror for body damage. The model of the used CW laser was of the fundamental mode with a Gaussian distribution. The model of the used pulsed laser was dominated by the fundamental mode that was mixed with some higher-order modes. The laser parameters are shown in Table 1. The targets used in the experiments were silicon-based and germanium-based flat window. The substrate material parameters are shown in Table 2.

Table 1. Laser parameters.

	Continuous Laser	Long-Pulse Laser	Short-Pulse Laser
Wavelength	1.06 μm	1.03 μm	1.06 μm
Maximum power/energy	2000 W	100 J	250 mJ
Pulse width	N/A	400 μs	10 ns
Gain medium	Nd:YAG	Yb:YAG	Nd:YAG

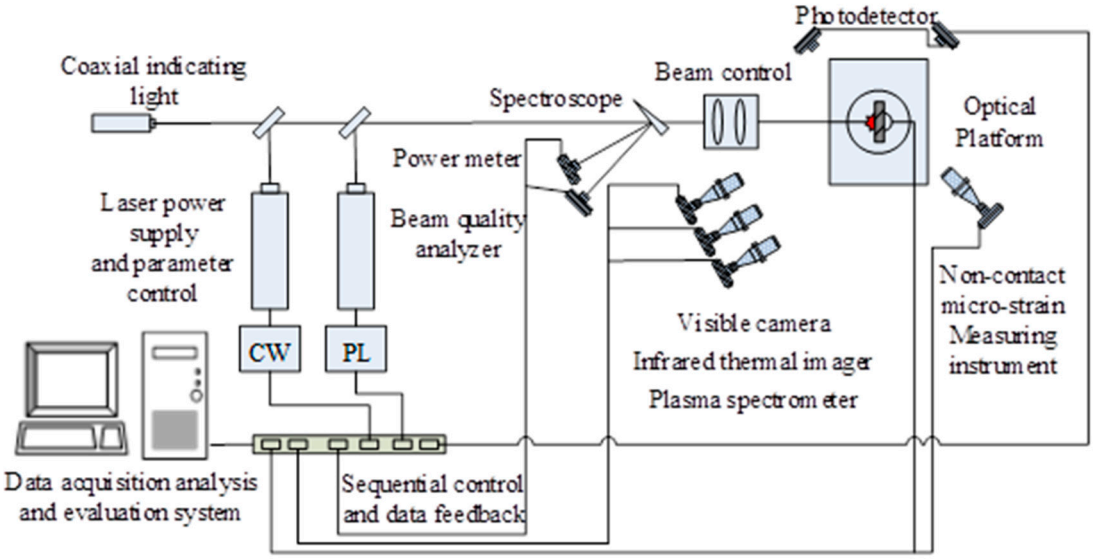

Figure 1. Laser damage effect experimental platform.

Table 2. Physical properties of substrate.

	Density (g/cm^3)	Specific Heat Capacity (J/(kg·k))	Thermal Conductivity (W/(m·k))	Coefficient of Linear Expansion (1/°C)	Anti-Reflection Coating Range
Germanium single crystal	5.33	310	59.8	5.4×10^{-6}	3–5 μm
Silicon single crystal	2.33	712	159	2.55×10^{-6}	2–6 μm

First, two kinds of window were used to measure the absorptivity. We used a 1.06 um continuous laser to irradiate the flat window and measuring the reflected power with a power meter, since the two substrates were not transparent to the Near-Infrared band; as such, the absorptivity shown in Table 3 could be obtained.

Table 3. Absorption rate of the 1.06 μm laser by a flat window.

	Silicon Broadband Window	Germanium Broadband Window
Incident laser power	20 W	20 W
Reflected laser power	13 W	14 W
Absorption rate	35%	30%

3.1. Continuous Laser Damage Flat Window Experiment

The continuous laser was used to verify the damage effect of the out-of-band laser on the flat window. Due to thermal stress deformation caused by laser irradiation, the spot of collimated light was shifted. The thermal deformation state of the flat window under continuous laser loading was observed with a scattering detection method—that shown in Figure 2a is before loading, that shown in Figure 2b is the spot shift caused by thermal distortion during loading, and that shown in Figure 2c is the spot shift before the lens body exploded.

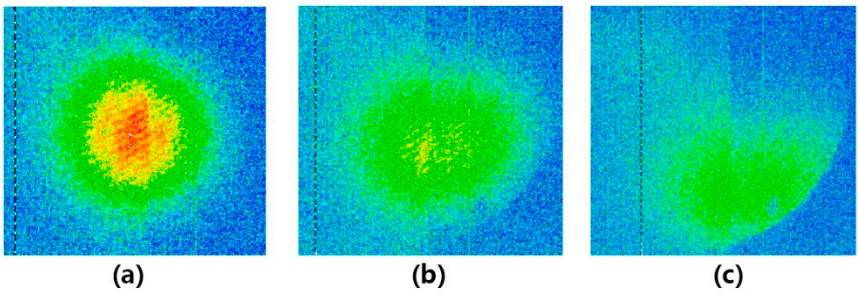

Figure 2. Changes in scattered light spots caused by thermal distortion. (**a**) Irradiation begins (**b**) Start to deform (**c**) Body explode.

By comparing the experimental results, it could be seen that the film color of the germanium window changed from 600 to 660 °C, and ripples were generated (Figure 3). At 660 °C, the film began to melt, and optical coating damage occurred. At 700 °C, substrate damage began. When the laser power reached 1500 W, the window body exploded. The film damage of the silicon window began to occur at 500 °C (Figure 4), and the damage of the film was similar to that of the germanium window mirror. When the laser power reached 1440 W, the substrate of the silicon window exploded at 950 °C.

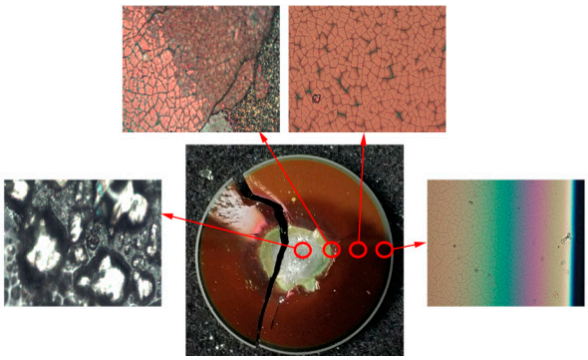

Figure 3. Damage of silicon broadband window (200×).

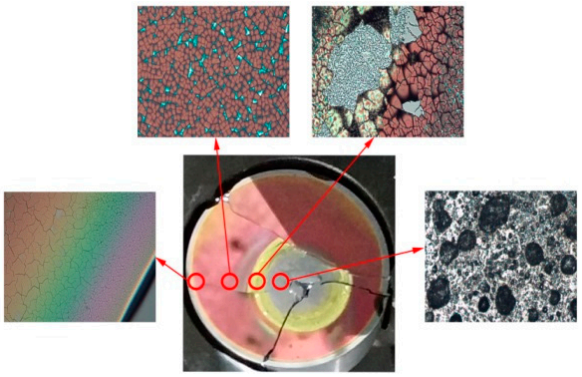

Figure 4. Damage of germanium broadband window (200×).

When the laser was irradiated to the flat window, due to the asymmetrical distribution of the high-power laser beam and non-uniform absorption, the temperature gradient and thermal stress in the material were caused. The larger temperature gradient and thermoelastic stress first appeared in the irradiated area, which made the window material generate thermal distortion. When the thermal stress gradually accumulated and exceeded the strength limit of the material, the irradiated area first burst, eventually causing macro damage to the window [26,27]. It can be seen from Table 4 that the damage thresholds of the NIR lasers out of band on the Ge and Si windows were close. The reason for the body damage was that the substrate absorption rate increased after the optical coating melted

and the temperature rose became faster, which caused substrate bursting. The damage of the optical film system was mainly caused by melting. It could be seen that the film system disappeared and the substrate was severely ablated when observed in the central area of irradiation. This was because when continuous laser light irradiated the surface of the window mirror, the thermal stability of the substrate material was better than that of the film. The thermal stress when the substrate was heated to 550–600 °C was not enough to cause the body damage of the window, but the optical film had begun to melt and be destroyed.

Table 4. Experimental results of the continuous laser.

Laser Power (W)	Silicon Window		Germanium Window	
	Peak Temperature (°C)	Damage Effect	Peak Temperature (°C)	Damage Effect
350	40	N/A	70	N/A
525	120	N/A	123	N/A
700	250	N/A	179	N/A
875	369	N/A	269	N/A
1050	558	N/A	374	N/A
1225	660	Optical Coating damage	544	Optical Coating damage
1440	740	Optical Coating damage	948	Substrate damage
1575	750	Substrate damage		

3.2. Long-Pulse Laser Damage Experiment

A long-pulse laser damage flat window experiment was performed. The absorption rates of a 1.03 μm laser for flat windows were measured. The measurement results are shown in Table 5. The absorption rate of the Si window for lasers in the 1.03 μm band was higher than that of the 1.06 μm band, and the absorption rate of the Ge window for lasers in the 1.03 μm band was slightly lower than the 1.06 μm band.

Table 5. Absorption rate of the 1.03 μm laser by a flat window.

	Silicon Broadband Window	Germanium Broadband Window
Incident laser power	6 W	6 W
Reflected laser power	3.5 W	4.3 W
Absorption rate	41.7%	28.3%

We performed a S-on-1 single-pulse experiment, loaded five pulses, and observed the experimental results, as shown in Table 6 below.

Table 6. Experimental results of the long-pulse laser.

Single-Pulse Energy (J)	Silicon Window Damage Effect	Germanium Window Damage Effect
3	N/A	N/A
6	N/A	N/A
11	N/A	Optical Coating damage
17	N/A	Optical Coating damage
23	N/A	Optical Coating damage
29	Optical Coating damage	Substrate damage
36	Optical Coating damage	Substrate damage
44	Substrate damage	Substrate damage
51	Substrate damage	Substrate damage
80	Substrate damage	Substrate damage

According to Table 6, when the laser energy reached 29 J, the Si window had coating damage, and at the same time, the plasma flash produced by the breakdown of electrons appeared in the irradiation area [28]. With the increase of energy, the damage of the optic film became more serious. The damage phenomenon is shown in Figures 5 and 6. When the energy reached 44 J, substrate damage occurred. When the energy reached 80 J, the first pulse caused substrate damage. When the laser energy reached 11 J, coating damage occurred in the Ge window. The coating damage became more serious at 17–23 J, and when the energy reached 29 J, the first pulse caused damage to the substrate. The long-pulse laser and continuous laser irradiation on windows were mainly caused by surface thermal fusion damage, and plasma absorption was the main cause of damage.

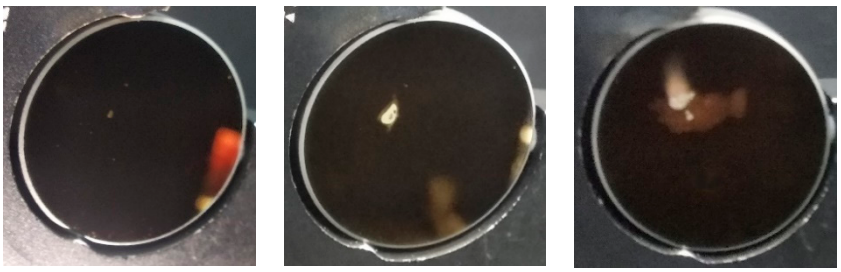

Figure 5. Damage phenomenon of the Ge window with long-pulse laser irradiation.

Figure 6. Damage phenomenon of the Si window with long-pulse laser irradiation.

3.3. Short-Pulse Laser Damage Experiment

A short-pulse laser damage window experiment was performed using the 1-on-1 method. The experimental results are shown in Table 7.

Table 7. Experimental results of the short-pulse laser.

Single-Pulse Energy (mJ)	Silicon Window Damage Effect	Germanium Window Damage Effect
65	N/A	N/A
90	N/A	N/A
115	Optical Coating damage	Optical Coating damage
135	Optical Coating damage	Optical Coating damage
160	Optical Coating damage	Substrate damage

Observing the damage phenomenon, it was found that, unlike the long-pulse damage, the coating damage caused by the short-pulse laser was shallower than that of the long pulse. Under the experimental conditions of this paper, only the Ge window showed slight substrate damage at the laser energy of 160 mj, though it showed no body damage (Figures 7 and 8). This was because the short-pulse laser damaged the material for a short time, mainly due to the effect of the laser electric field, so it mostly appeared as film damage. Non-linear effects (such as non-linear absorption, non-linear refractive index, and self-focusing effects) induced by high electric fields when the high-power lasers acted on the windows were the main causes of damage. Since the laser intensity in the short-pulse laser irradiation area reached the order of GW/cm^2, the self-focusing effect appeared. By combining

the above three experimental results, it could be seen that short-pulse lasers outside the band could only cause mild film damage, while long-pulse lasers could cause body damage.

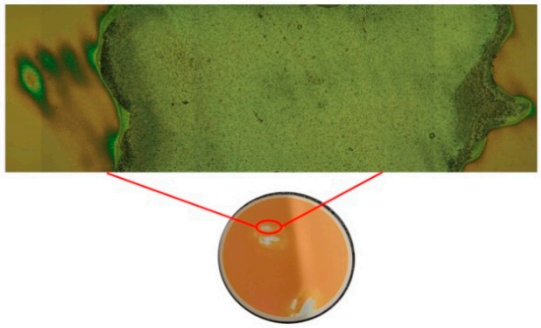

Figure 7. Damage phenomenon of the Si window with short-pulse laser irradiation.

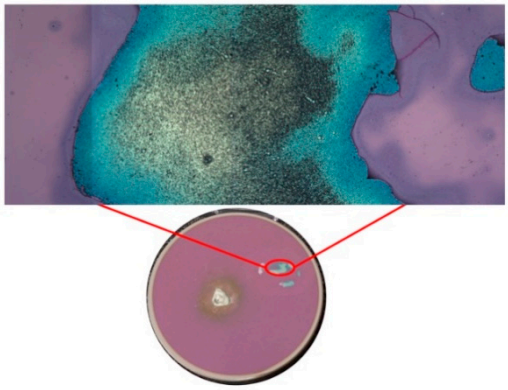

Figure 8. Damage phenomenon of the Ge window with short -pulse laser irradiation.

3.4. Composite Laser Damage Experiment

According to the results of the pulse laser damage to the window, although the short-pulse laser had a higher peak power, it did less damage to the window and had difficulty damaging the substrate. Therefore, this paper used a combination of a long-pulse and a CW laser to perform the damage experiment. The trigger time of the long-pulsed laser was controlled by digital delay pulse generator. When the current temperature of the thermal imager reached a preset value, the CW laser was turned off and the pulsed laser was triggered at the same time. The results of the composite laser experiment are shown in Tables 8 and 9 below.

Table 8. Damage phenomenon of the Ge window by the composite laser.

Single-Pulse Energy (J)	Continuous Laser Heating Temperature	Germanium Window Damage Effect
2	100	N/A
2	145	Optical Coating damage
3	80	N/A
3	100	Optical Coating damage
3	160	Optical Coating damage
3	220	Substrate damage

The damage phenomenon is shown in Figures 9 and 10. It could be seen from the experimental results of the Ge window that the composite laser could cause slight damage to the film system at the laser energy of 2 J and 145 °C. The results of the Si window experiments showed that the composite laser started to damage the optic film system at 17 J. When the pulsed laser energy is less than 17j, the continuous laser pre-heating temperature needs to exceed 300 °C to cause mild film damage,

which was consistent with the long-pulse laser damage mechanism discussed above. Increasing the continuous laser preheating temperature while maintaining the pulse laser energy at 17 J led to more serious optic film damage, and the substrate damage was caused when the preheating temperature reached 260 °C.

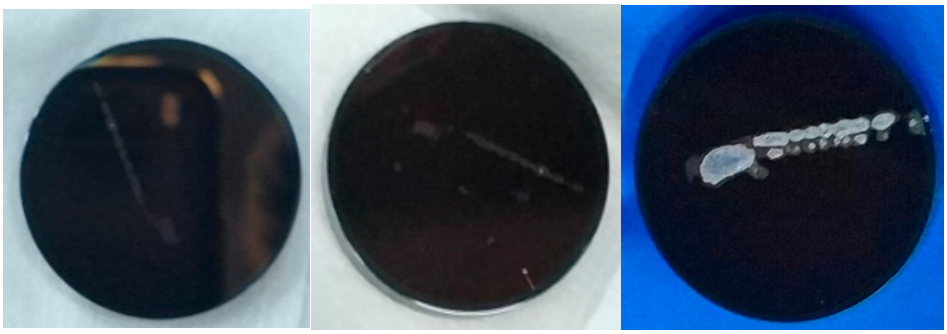

Figure 9. Damage phenomenon of the Ge window by the composite laser.

Table 9. Damage phenomenon of the Si window by the composite laser.

Single-Pulse Energy (J)	Continuous Laser Heating Temperature	Germanium Window Damage Effect
11	100	N/A
11	200	N/A
11	310	Optical Coating damage
17	100	Optical Coating damage
17	120	Optical Coating damage
17	168	Optical Coating damage
17	210	Optical Coating damage
17	266	Substrate damage

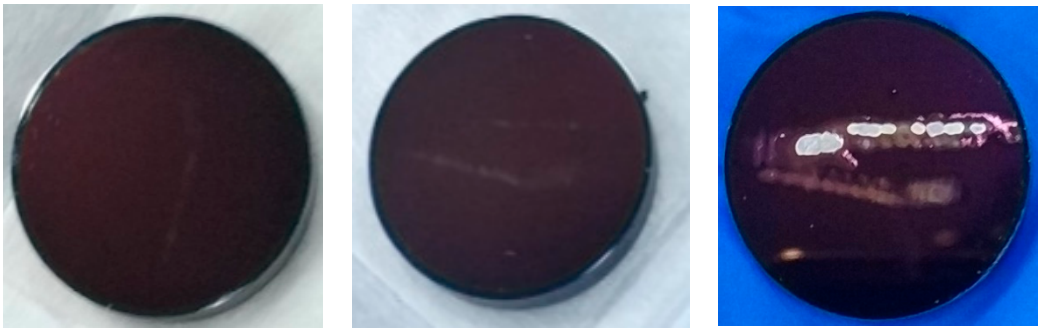

Figure 10. Damage phenomenon of the Si window by the composite laser.

Table 10 summarizes the damage threshold data for different lasers. The giant-pulse laser waveform used in this experiment was of the spike and square mixed waveform. The energy of the spike pulse as about three-to-four times that of the square pulse. After the flat window was pre-heated by continuous light, the spike pulse part first acted on the window body. Its high peak energy was absorbed by the optical film and substrate. The optical film was instantly melted under the double temperature rise effect, and the residual energy was directly absorbed by the substrate and eventually caused damage to the substrate.

Table 10. Comparison of the damage thresholds of different lasers.

	Si Window		Ge Window	
	Coating Damage	**Substrate Damage**	**Coating Damage**	**Substrate Damage**
Continuous laser (kW/cm^2)	1.56	1.83	1.56	2
Long-pulse laser (J/cm^2)	45	64.9	14	36.9
Composite laser (J/cm^2)	14	21.6	2.55	3.8

4. Conclusions

(1). Out-of-band high-energy lasers can damage Ge and Si windows. NIR laser damage to Ge and Si windows with medium wave Anti-Reflection coatings occurred at 500–600 °C The damage thresholds of the NIR continuous laser and the pulsed laser to the Ge window were divided into 2 kW/cm^2 and 37 J/cm^2, respectively, and the damage thresholds of the NIR continuous laser and pulsed laser to the Si window were divided into 1.8 kW/cm^2 and 65 J/cm^2. The high-energy laser damage mechanism of long-pulse laser and CW laser is mainly manifested as thermal effect, and it is easier to damage the substrate. The damage mechanism of the short-pulse laser as a high-power laser was mainly manifested by the laser electric field effect, but it was difficult to damage the substrate due to the laser's low energy.

(2). The pulse-continuous composite laser could effectively improve the damaging effect, and the long-pulse laser energy had a significant effect on the damage. The thresholds of the damage to the substrate by the composite laser were 21.6 J/cm^2 for the silicon-based flat window and 3.8 J/cm^2 for the germanium-based flat window.

Author Contributions: L.Y. and L.L. write the original draft. T.W. and S.J. (Shao Junfeng) are responsible for collating experimental data. L.X. and S.J. (Sun Junjie) revised and edited the manuscript. S.M. and C.X. provided resource support for the research. All authors have read and agreed to the published version of the manuscript.

Funding: The work reported in this paper is supported by the National Key Laboratory of laser matter interaction (Grant No. SKLLIM1904) and the Youth Innovation Promotion Association of Chinese Academy of Sciences (Grant No. 2018248/Y80139C) and "Xuguang" Talent Program of Changchun Institute of Optics and Machinery, Chinese Academy of Sciences (Grant No. 201900X).

Conflicts of Interest: The authors declare no conflict of interest.

References

1. Qiu, D.D.; Zheng, Z.; Wang, R.; Jiang, T.; Cheng, X.A. Mechanism research of pulsed-laser induced damage to CCD imaging devices. *Acta Opt. Sin.* **2011**, *31*, 0214006.
2. Zhiwu, Z.; Zhen, Z.; Xiang'ai, C.; Liangjin, H.; Zejin, L. Damage phenomenon and probability of CCD detectors under single-laser-pulse irradiation. *Infrared Laser Eng.* **2013**, *42*, 113–118.
3. Tian, J. The carrier transportation of photoconductive HgCdTe detector irradiated by CW band-off laser. *J. Infrared Millim. Waves* **2012**, *31*, 216–221.
4. Li, X.Q.; Cheng, X.A.; Wang, R.; Ma, L.Q.; Lu, Q.S. Investigation of thermal effect of HgCdTe Detector with irradiation by off-band CW CO_2 laser. *Chin. J. Lasers* **2003**, *30*, 1070–1074.
5. Wang, R.; Si, L.; Lu, Q.S.; Liu, Z.J. Experiment study on HgCdTe (PC type) detector system irradiated by laser out of response waveband. *Laser Infrared* **2003**, *5*, 5.
6. Li, L.; Qisheng, L. Numerical simulation of dynamic response of PC-Type HgCdTe detector irradiated by in-band and out-of-band laser beams. *Acta Opt. Sin.* **2008**, *28*, 1952–1958. [CrossRef]
7. Xin, Z.; Tian, J.; Xiang-Ai, C.; Hou-Man, J.; Qi-Sheng, L. A new phenomenon of photoconductive InSb detector under the irradiation of out-band laser. *Acta Phys. Sin.* **2012**, *4*, 61.
8. Fei, W. Damage Mechanisms of Laser on PV Type Single Element HgCdTe Device and Visible-Light CCD. Master's Thesis, National University of Defense Science and Technology, Changsha, China, 2006.
9. Wang, R.; Cheng, X.A.; Lu, Q. Experimental study on damage to detector system of three HgCdTe (PC type) units irradiated by CW 3.8μm laser. *High Power Laser Part. Beams* **2004**, *16*, 31–34.

10. Yong, C.; Mengzhen, Z.; Yunfeng, M.; Jingsong, W.; Xu, L.; Fangzheng, D.; Chaoyong, T.; Xia, C.; Yanlong, G.; Hua, C. Mechanism and effects of complex laser ablation. *Infrared Laser Eng.* **2016**, *45*, 1105005. [CrossRef]
11. Wang, Q.; Bo, P.; Zhang, Y.; Hu, W.; Li, Z. Damage mechanism of aluminum by long-short composite pulsed laser. *Laser Optoelectron. Prog. Infrared Laser Eng.* **2018**, *10*, 55.
12. Luguang, J.; Guomin, Z.; Minsun, C. Investigation on the irradiation effects of Q235 steel targets by combined laser. *Infrared Laser Eng.* **2011**, *40*, 848–852.
13. Xiao, J.; He, H.; Xia, H.; Jia, J. Temperature flied simulation on aluminium alloy irradiated by long pulsed laser and continuous wave laser. *Chin. J. Lasers* **2012**, *39*, 1103002–1103006. [CrossRef]
14. Xiao, J.; He, H.; Xia, H. Stress simulation of aluminum alloy irradiated by long pulsed laser and continuous wave laser. *Chin. J. Lasers* **2013**, *8*, 40.
15. Fang, X.; Yuan, S.; Liu, W.; Yan, B.; Huang, B. Absorption measurement of optical thin films under high power density with a Closed Cavity. *Chin. Opt. Lett.* **2015**, *13*, 033101. [CrossRef]
16. Xu, C.; Yi, P.; Fan, H.; Qi, J.; Qiang, Y.; Liu, J.; Tao, C.; Li, D. Correlations between the oxygen deficiency and the laser damage resistance of different oxide films. *Appl. Surf. Sci.* **2014**, *289*, 141–144. [CrossRef]
17. Wang, Y.; Ma, Y.; Wang, D.; Su, C.; Zhang, X.; Li, C. Theoretical simulation analysis of long-pulse laser induced damage in a BK7:SiO2/HfO2 optical anti-reflective films. *Optik.* **2018**, *156*, 530–535. [CrossRef]
18. Ling, X.; Wang, G.; Zhao, Y.; Shao, J.; Fan, Z. Laser-induced damage of the optical films prepared by electron beam evaporation and ion beam sputtering in vacuum. *Optik* **2014**, *125*, 6474–6477. [CrossRef]
19. Tan, T.T.; Liu, B.J.; Wu, Z.H.; Liu, Z.T. Annealing effects on structural optical properties and laser-induced damage threshold of MgF2 thin films. *Acta Metall. Sin. (English Letters)* **2017**, *30*, 73–78. [CrossRef]
20. Melnikas, S.; Tolenis, T.; Smalakys, L.; Batavičiūtė, G.; Melninkaitis, A.; Kičas, S. Enhancement of laser-induced damage threshold in chirped mirrors by electric field reallocation. *Opt. Express* **2017**, *25*, 26537–26545. [CrossRef]
21. Allmen, M.V.; Blatter, A. *Laser-Beam Interactions with Materials: Physical Principles and Applications*; Springer: Berlin/Heidelberg, Germany, 1995.
22. Theodore, L.; Adrienne, S. *Fundamentals of Heat and Mass Transfer*; John Wiley & Sons: New York, NY, USA, 2011.
23. Lee, K.H.; Shin, W.S.; Kang, E.C. Analysis of optical damage in germanium induced by a continuous wave laser. *Appl. Opt.* **2013**, *52*, 2055–2061. [CrossRef]
24. Malik, R.; Mills, B.; Price, J.H.; Petrovich, M.; Moktadir, Z.; Li, Z.; Rutt, H.N. Determination of the mid-IR femtosecond surface-damage threshold of germanium. *Appl. Phys. A Mater. Sci. Process.* **2013**, *113*, 127–133. [CrossRef]
25. Wu, C.W.; Wang, J.; Huang, C.G. A coupled model on energy conversion in laser power beaming. *J. Power Sources* **2018**, *393*, 211–216. [CrossRef]
26. Ge, J.M.; Su, J.H.; Xu, J.Q. Application of laser-induced breakdown spectroscopy to analysis of thin-film damage. *Acta Photonica Sin.* **2016**, *4*, 45.
27. Zhu, L.; Yang, D.; Wang, L.; Zeng, J.; Zhang, Q.; Xie, M.; Zhang, P.; Dai, S. Optical and thermal stability of Ge-as-Se chalcogenide glasses for femtosecond laser writing. *Opt. Mater.* **2018**, *85*, 220–225. [CrossRef]
28. Su, J.; Lv, N.; Ge, J. Characteristics of plasma shock waves in laser-induced film damage. *Chin. J. Lasers* **2016**, *12*, 43.

© 2020 by the authors. Licensee MDPI, Basel, Switzerland. This article is an open access article distributed under the terms and conditions of the Creative Commons Attribution (CC BY) license (http://creativecommons.org/licenses/by/4.0/).